

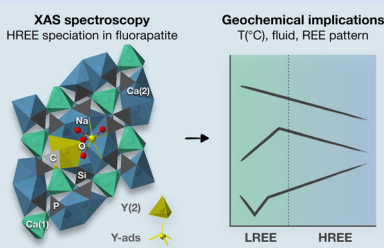
Sorption model for yttrium in fluorapatite: Geochemical implications

C. Bonnet^{1,2*}, M. Muñoz¹, O. Mathon², V. Motto-Ros³,
A. Elghali⁴, F. Parat¹, J. Aubineau¹, J.-L. Bodinier^{1,4}



<https://doi.org/10.7185/geochemlet.2326>

Abstract



Fluorapatite (FAP), which occurs in various geological settings, contains rare earth elements (REE) for which unveiling the crystal chemistry is a key geochemical issue, especially for unravelling the conditions of fractionation and crystallisation. However, no consensus has been reached regarding their binding modes in FAP, with studies suggesting REE³⁺-Ca²⁺ substitution at the Ca(1) site, or at the Ca(2) site, or involving adsorption mechanisms. Our contribution here is based on yttrium K-edge X-ray absorption spectroscopy (XAS), performed on two genetically contrasting minerals: a hydrothermal FAP (from Durango, Mexico), and a sedimentary phosphorite (from Morocco). The results clearly show that Y substitutes for the Ca(2) site in both FAP.

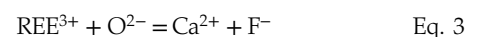
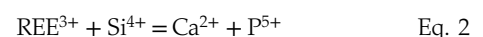
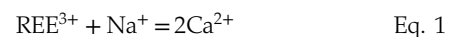
However, the spectral differences observed for the sedimentary FAP (B-type carbonated-FAP) suggest a sorption model that is either i) a mixture of Y-Ca(2) substitution and Y-adsorbed as an inner shell complex, or ii) Y-Ca(2) substitution along with carbonate groups replacing phosphate groups in the surrounding atomic shell. These models of yttrium sorption in FAP shed new light on the understanding of rare earth partitioning and enrichment processes, with major geochemical implications such as i) the identification of crystallising fluids and temperature in magmatic-hydrothermal settings, and ii) preservation of past seawater-porewater conditions in sedimentary settings.

Received 12 December 2022 | Accepted 12 July 2023 | Published 25 August 2023

Introduction

Fluorapatite (FAP; Ca₅(PO₄)₃F) is an accessory mineral that hosts significant amounts of rare earth elements (REE, including yttrium) from ~200 to 20,000 ppm (Emsbo *et al.*, 2015), where Y exhibits similar behaviour to heavy rare earth elements (HREE, from Gd to Lu) and is therefore associated with them. For Earth Sciences, REE normalised patterns in FAP are proxies to i) reconstruct partitioning models and determine partition coefficients (Blundy and Wood, 2003), ii) identify the source fluids, their chemical composition and their REE complexation (Mackie and Young, 1973; Krneta *et al.*, 2018), iii) characterise the deposition/crystallisation conditions such as temperature, pH, redox (Chen *et al.*, 2002; Kocsis *et al.*, 2016), and iv) reveal the potential late diagenetic or hydrothermal alterations (Reynard *et al.*, 1999; Cherniak, 2000). The crystal chemistry of REE in FAP also controls its partitioning and normalised patterns (Blundy and Wood, 2003). In addition, it can potentially provide valuable insight into the crystallisation conditions such as temperature (Khudolozhkin *et al.*, 1973; Pan and Fleet, 2002 and references therein), fluids (Mackie and Young, 1973) or diffusion (Cherniak, 2000). However, determining the sorption models of REE is not systematically well constrained and is at the heart of many studies since FAP can potentially integrate REE in two

distinct crystallographic Ca sites, namely the 9 fold coordinated Ca(1) and the 7 fold coordinated Ca(2) sites (Hughes *et al.*, 1991) (Fig. S-1a, b), and can also show nano-crystallinity typically observed in sedimentary deposits (Aubineau *et al.*, 2022) that may favour adsorption mechanisms and apparent no-fractionation behaviour (Reynard *et al.*, 1999). In order to maintain electroneutrality, each of the above sorption models may involve coupled substitutions such as (Pan and Fleet, 2002 and references therein):



In a study based on ligand type, Urusov and Khudolozhkin (1974) suggested that light (L)REE preferentially occupy the more covalent Ca(1) position, while HREE display preference for the more ionic Ca(2) position. Conversely, X-ray diffraction structure refinements on synthetic REE-doped FAP suggest that LREE are favoured in Ca(2) while HREE are favoured in Ca(1) (Hughes *et al.*, 1991; Fleet and Pan, 1995). Moreover, Borisov and Klevtsova (1963) have demonstrated that

1. Geosciences Montpellier, Université de Montpellier, CNRS, Montpellier, France
2. ESRF, European Synchrotron Radiation Facility, Grenoble, France
3. ILM, Institut Lumière Matière, Université Claude Bernard Lyon 1, Lyon, France
4. GSMI, Geology and Sustainable Mining Institute, Mohammed VI Polytechnic University, Ben Guerir, Morocco

* Corresponding author (Email: clement.bonnet02@etu.umontpellier.fr)



substitutions of both LREE and HREE for Ca occurred only at the Ca(2) site which was confirmed by EPR (Electron Paramagnetic Resonance) spectroscopy (Chen *et al.*, 2002). In natural marine environments, Kashiwabara *et al.* (2018) proposed that deep sea muds mostly trap REE by adsorption onto FAp crystals. Similarly, Reynard *et al.* (1999) conclude that the REE adsorption is likely to occur in the case of sedimentary/biogenic FAp.

To contribute to the understanding of the crystal chemistry of REE, and more specifically HREE in FAp and geochemical implications that follows, we propose a direct characterisation of the yttrium speciation (*i.e.* fixation modes, coupled substitutions and crystallographic preferences) using X-ray absorption spectroscopy (XAS) at the Y K-edge. XANES (X-ray absorption near edge structure) and EXAFS (extended absorption near edge structure) spectra are analysed by quantitative refinements, linear combinations and wavelet analysis (Muñoz *et al.*, 2003). This study focuses on two representative and genetically contrasting natural FAp: i) of hydrothermal origin (H-FAp) from Durango, Mexico, and ii) of sedimentary origin (S-FAp) from Moroccan phosphorites, and mainly composed of B-type carbonated FAp (*i.e.* FAp showing carbonate-phosphate substitutions).

Yttrium Speciation in Model Compounds

Two model compounds, Y_2O_3 and synthetic Y-adsorbed FAp (Y-ads), were studied and used for qualitative and quantitative analysis of spectroscopic data. Their normalised XANES and EXAFS spectra show contrasting spectral signatures (Fig. 1a and b, respectively). For both compounds, the wavelet analysis of the EXAFS spectra (Fig. 2a and b, respectively) shows a maximum of the 1st neighbours' amplitude (*i.e.* $(R + \Phi) = 1.75 \text{ \AA}$) localised around 5.5 \AA^{-1} . For Y_2O_3 , the second and third shells are significantly shifted at higher k (wavenumber) values due to the presence of yttrium (Fig. 2a). However, the presence of oxygen in these shells moderates the shift of the amplitude term (maximum $\sim 7.5 \text{ \AA}^{-1}$), showing a strong asymmetric shape due to the distribution of Y, O and Y at distances of 3.53(4), 4.02(3) and 4.01(5) \AA , respectively (Table 1).

Regarding Y-ads, the EXAFS shell fitting reveals the presence of 8.1(8) oxygen 1st neighbours located at 2.38(1) \AA (Fig. 2b,

Table 1), which is consistent for Y-adsorbed species (Ragnarsdottir *et al.*, 1998). Additionally, the best fit is obtained with two Ca as 2nd neighbours at 2.98(2) \AA , suggesting a tridentate ionic bonding with the FAp crystal surface in the c axis channel. Note that in such a configuration (Fig. 3b), a typical O–Y–O angle of about 73° , characteristic of the regular 8 fold polyhedron, is preserved (Ni *et al.*, 1995). The 3rd shell observed on the wavelet modulus (Fig. 2b) shows a contribution at high k values ($\sim 8.5 \text{ \AA}^{-1}$), which is in agreement with the presence of one Y fitted at 3.87(3) \AA (Table 1). The latter probably results from Y pairs adsorbed on a single c axis channel, consistent with the formation of Y polyatomic species or Y polymerisation in water (Ragnarsdottir *et al.*, 1998).

Yttrium Speciation in Hydrothermal Fluorapatite

The shell fitting performed on the EXAFS spectrum of hydrothermal FAp (H-FAp) reveals the presence of 7.0(7) oxygen located at 2.37(2) \AA (Table 1), confirming that Y integrates the FAp crystal lattice within the 7 fold coordinated Ca(2) site by a substitution mechanism (hereafter referred to as Y(2); Fig. 3a). The fitted next nearest neighbour environment around Y, which consists of 5 P distributed between 3.09(1) and 3.70(1) \AA , and 10 Ca at an average distance of 4.16(1) \AA (Table 1), shows consistency with the theoretical Ca(2) atomic landscape (Tables 1, S-1b). In contrast, the radial distribution function around Ca(1) shows an intense peak in the Fourier transform (FT) magnitude (see *ab initio* EXAFS calculations and corresponding FT in Fig. S-2), due to the presence of 2 Ca located as close as 3.42 and 3.45 \AA (Table S-1a). This feature appears strongly incompatible with the yttrium atomic landscape observed and successfully fitted in H-FAp (Fig. 2c, Table 1).

The lack of a high k contribution in the next nearest environment around Y eliminates the hypothesis of a coupled substitution involving a second heavy trivalent cation such as REE plus a vacancy (*i.e.* Eq. 4). Thus, the charge compensation is likely to meet the assumptions presented in Equations 1, 2 and 3, although these cannot be formally verified since the contrast in atomic number and coordination number (CN) between,

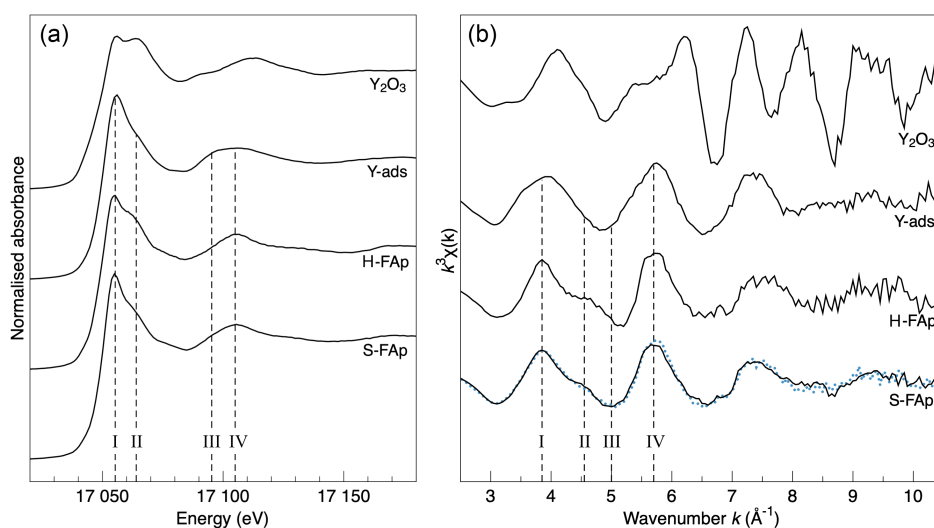


Figure 1 X-ray absorption spectra collected at the Y K-edge for Y_2O_3 and Y-ads FAp model compounds, and H-FAp and S-FAp samples. (a) Normalised XANES spectra, (b) k^3 -weighted EXAFS spectra. Roman numerals (I to IV) refer to characteristic spectral features. Blue dotted line represents the linear combination fit (LCF) result based on Y-ads and H-FAp components, suggesting a mixture of 59 % Y substituted at the Ca(2) site and 41 % of adsorbed Y for S-FAp.

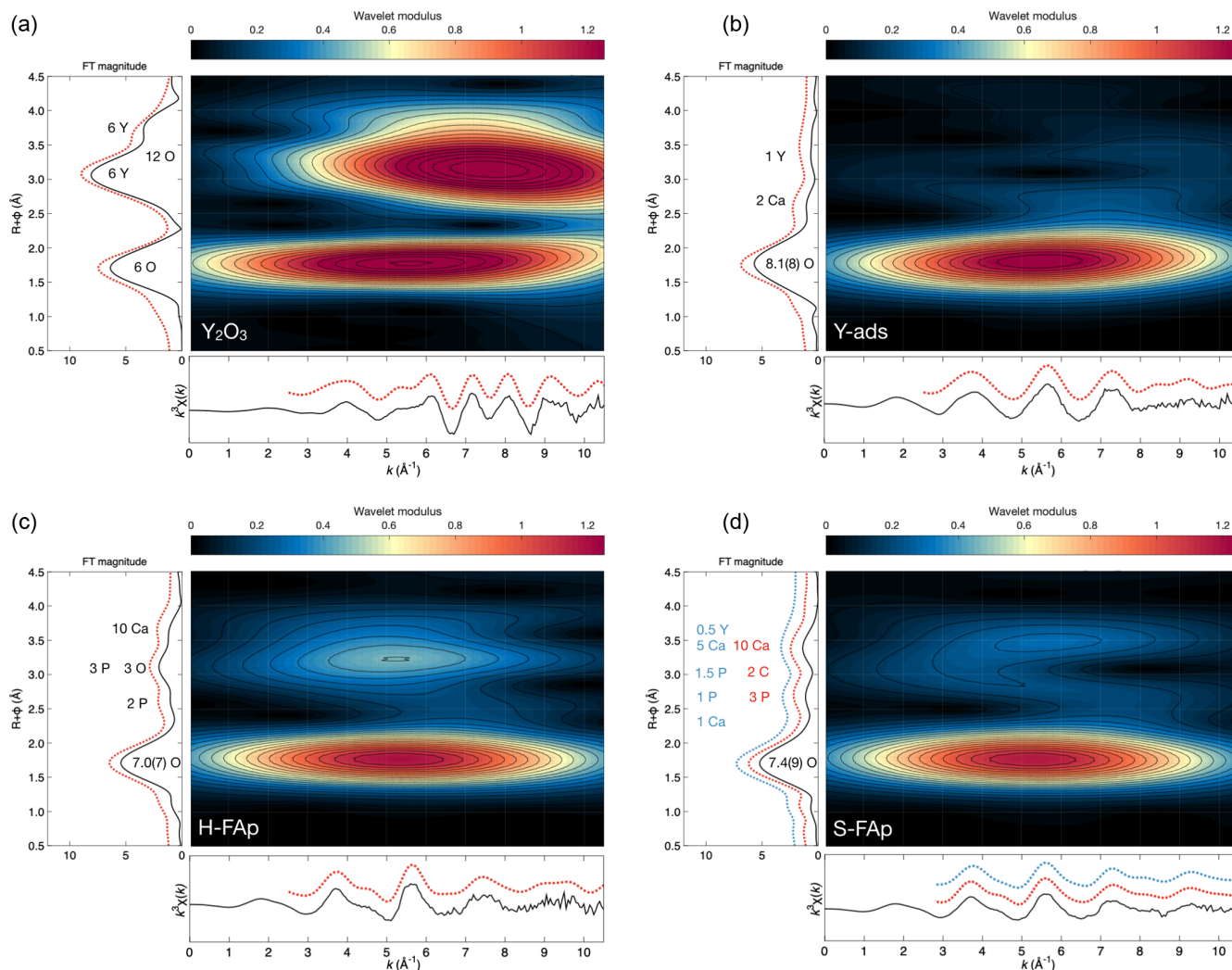


Figure 2 Wavelet transform analysis of EXAFS spectra with corresponding k^3 -weighted EXAFS spectra and Fourier transform (black solid lines). Results of multi-shell fits are shown in both the k - and R -spaces (shifted dotted lines), (a) Y_2O_3 , (b) Y-ads, (c) H-FAp, (d) S-FAp with the mixed “Y(2) + Y-ads” model in blue and the “Y(2) + carbonate” model in red.

respectively, Na and Ca, Si and P, and O and F are too subtle to be distinguished.

Yttrium Speciation in Sedimentary Fluorapatite

The fit of the S-FAp EXAFS spectrum provides, for the 1st atomic shell, an average coordination of 7.4(9) (Table 1), which is slightly higher than that obtained for H-FAp, but within the margin of error. We also note on the wavelet modulus of S-FAp (Fig. 2d), a major difference in the 3rd neighbour shell, at $(R + \Phi) \approx 3.25$ Å (Fig. 2c), where a clear contribution arising from 3 P and 3 O (at 3.39 and 3.67 Å, respectively) is observed for H-FAp, but absent for S-FAp. To interpret these discrepancies, we propose two distinct structural models that were successfully fitted (Table 1, Fig. 2).

The first one (blue dotted lines in Fig. 2d) involves a mixture of two speciation models: a Y(2) substitution and an inner shell Y adsorption, the latter tending to decrease the intensity of the contribution located at $(R + \Phi) \approx 3.25$ Å. Note that a mixture with Y(1) results in a failed fit and is therefore excluded given the absence of its typical contribution of Ca located at ~ 3.43 Å

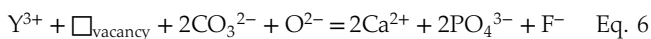
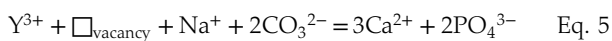
(Figs. S-1a, S-2b, Table S-1a; $(R + \Phi) \approx 3$ Å in Fig. 2c and d). Additionally, different features of the XANES and EXAFS spectra tend to corroborate such a scenario (Fig. 1). Among them, the maximum of the white line (feature I in Fig. 1a) is significantly higher for Y-ads compared to H-FAp, while it shows an intermediate value for S-FAp. In accordance, the linear combination fit (LCF) of the EXAFS spectrum (Fig. 1b) also suggests a mixture of Y(2) and Y-ads.

The second model (red dotted lines in Fig. 2d) rather implies Y(2) together with two concomitant carbonate groups (CO_3^{2-} replacing two phosphate groups (PO_4^{3-}) in the 3rd atomic shell. The presence of carbon in the neighbouring of yttrium causes the decrease in intensity of the $(R + \Phi) \approx 3.25$ Å contribution; light elements (C) having lower back scattering amplitudes than heavier elements (P). This model is in perfect agreement with i) the nature of S-FAp, which is identified as B-type carbonate-FAp (Figs. S-5, S-6), and ii) the location of structural carbonate groups, as determined by high resolution transmission electron microscopy on B-type carbonate-FAp (Kis *et al.*, 2019). Such a “Y(2) + carbonate” model implies a significant distortion of the crystal lattice (Table 1) and a co-location of C and REE, which is consistent with the results of Liao *et al.* (2019) in analogous samples. In this case, the excess

Table 1 EXAFS fitting results for selected Y-standards and natural FAp samples and corresponding theoretical structural model. CN stands for the coordination number, R for the radial distance, σ^2 for the Debye-Waller factor and Δc_3 for the anharmonic parameter. The estimated parameters have uncertainty values in brackets, while fixed parameters do not. Linked estimated parameters share one of these superscript symbols: +, ++, *, **. Theoretical structures references: (1) Faucher and Pannetier (1980); (2) Ni *et al.* (1995); (3) Hughes *et al.* (1990).

Fitted sample	Theoretical model of local structure applied to fit				Multiple shell fitting				Fit information and statistics		
	Cluster	Path	CN	R (Å)	CN	R (Å)	σ^2 (Å ⁻²)	Δc_3 (Å ⁻³)	Fitted parameters	Degree of freedom	R-factor (%)
Y ₂ O ₃	Y ₂ O ₃ ⁽¹⁾	Y-O ₁	6.0	2.28	6.0	2.30 (1)	0.008 (2)		8	17	1.9
		Y-Y ₁	6.0	3.55	6.0	3.54 (4)	0.003 (1)				
		Y-Y ₂	6.0	4.05	6.0	4.01 (5)	0.004 (2)				
		Y-O _{2,3}	12.0	4.09	12.0	4.02 (3)	0.009 (2)				
Y-ads	Y adsorbed ^(2,3)	Y-O ₁	8.0	2.38	8.1 (8)	2.38 (1)	0.008 (1)	0.0007 (2)	8	17	2.9
		Y-Ca ₁	2.0	2.96	2.0	2.96 (2)	0.011 (2)				
		Y-Y ₁	1.0	3.87	1.0	3.87 (3)	0.006 (3)				
		Y-O ₁	7.0	2.44	7.0 (7)	2.37 (2)	0.008 (1)	0.0015 (4)			
H-FAP	Ca(2)FAp ⁽³⁾	Y-P ₁	1.0	3.08	1.0	3.09 (1) ⁺	0.002 (1) [*]		10	17	0.95
		Y-P ₂	1.0	3.26	1.0	3.28 (1) ⁺	0.002 (1) [*]				
		Y-O _{2,3}	3.0	3.35	3.0	3.40 (4) ⁺⁺	0.015 (6) ^{**}				
		Y-P ₃	1.0	3.49	1.0	3.51 (1) ⁺	0.002 (1) [*]				
		Y-P ₄	2.0	3.68	2.0	3.70 (1) ⁺	0.002 (1) [*]				
		Y-Ca _{1,2}	10.0	4.03	10.0	4.16 (1)	0.015 (1)				
		Y-O ₁	7.5	2.44	7.4 (9)	2.38 (4)	0.009 (2)	0.0017 (7)			
		Y-Ca ₁	1.0	2.96	1.0	2.98 (2)	0.008 (3)				
S-FAP (1 st fit)	Ca(2)FAp ⁽³⁾ + Y adsorbed ^(2,3)	Y-P _{1,2}	1.0	3.17	1.0	3.16 (6) ⁺	0.006 (8) [*]		10	17	1.3
		Y-P ₃	0.5	3.49	0.5	3.49 (6) ⁺	0.006 (8) [*]				
		Y-P ₄	1.0	3.68	1.0	3.68 (6) ⁺	0.006 (8) [*]				
		Y-Y ₁	0.5	3.87	0.5	4.06 (2) ⁺⁺	0.014 (3) ^{**}				
		Y-Ca _{1,2}	5.0	4.03	5.0	4.12 (2) ⁺⁺	0.014 (3) ^{**}				
		Y-O ₁	7.0	2.44	7.4(9)	2.38 (4)	0.009 (2)	0.0017 (7)			
S-FAP (2 nd fit)	Ca(2) B-type FAp ⁽³⁾	Y-P _{1,2}	2.0	3.17	2.0	3.14 (2) ⁺	0.008 (3) [*]		11	17	0.4
		Y-P ₃	1.0	3.49	1.0	3.36 (2) ⁺	0.008 (3) [*]				
		Y-C ₄	2.0	3.68	2.0	3.47 (4)	0.005 (7)				
		Y-Ca _{1,2}	10.0	4.03	10.0	4.24 (6)	0.019 (3)	0.0023 (9)			

of charge of Y³⁺ could be balanced according to the following equations:



where the vacancies likely refer to Ca(2) sites, and sodium, fluorine or carbonates are most often in excess relative to rare earth elements. However, it is not possible to formally distinguish these two hypotheses using the approach proposed here, and further *in situ* characterisation at the micrometric scale is required.

Geochemical Implications

In accordance with the crystal lattice strain partitioning model, it is proposed that the partition coefficient of REE in magmatic-hydrothermal FAp originates from the crystallographic preference of HREE for the Ca(1) site, and LREE for the Ca(2) site (Hughes *et al.*, 1991). However, in the case of Durango FAP, we clearly point out that Y substitutes for Ca in the Ca(2) site.

This could suggest that a partition model involving the Ca(1) site for HREE is not appropriate for the Durango FAP, where a HREE-depleted normalised pattern (Fleet and Pan, 1995) could rather reflect the progressive ionic incompatibility of REE for the Ca(2) site along the lanthanide series. These assumptions should be taken with caution given that the Durango FAP does not prevail for all other FAP, and given that REE patterns may vary significantly depending on the fluid conditions (Krneta *et al.*, 2018). Indeed, it is possible that the Durango H-FAP undergoes geochemical processes that favour Ca(2), as diffusion of REE in the Ca(2) site through the c axis channel may occur during thermal events (Cherniak, 2000). Furthermore, the different complexation modes in solution play a role in the distribution of REE between Ca(2) and Ca(1) sites involving Na or Si coupled substitutions (Mackie and Young, 1973). For example, the preference of REE for Ca(2) decreases with increasing Si content or temperature in the 700–1200 °C range (Khudolozhkin *et al.*, 1973; Pan and Fleet, 2002 and references therein). This could confirm that the Durango FAP was more likely formed at a medium temperature with saline fluids, in agreement with the literature (Gleason *et al.*, 2000 and references therein).



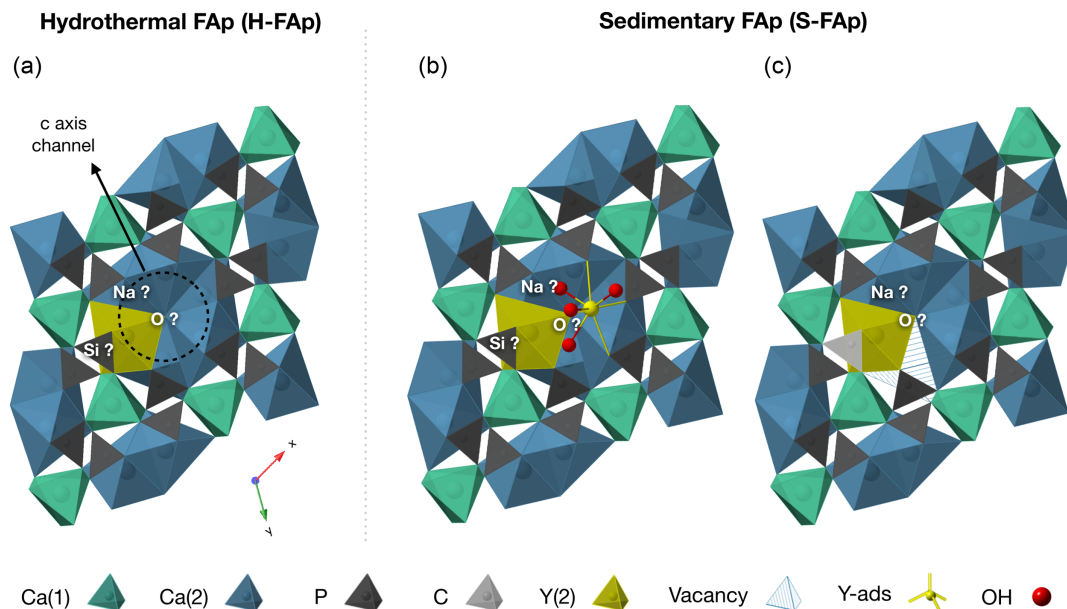


Figure 3 Fluorapatite crystal structure projected along c axis showing yttrium speciation models, (a) H-FAP: substitution at the Ca(2) site, (b) S-FAP: mixture of substitution at the Ca(2) site together with an inner shell adsorption at the c axis channel, (c) S-FAP: substitution at the Ca(2) site with concomitant C replacing P and Ca vacancy. Si, Na and O labels indicate potential coupled substitutions required to compensate the excess of electronic charge due to Y^{3+} - Ca^{2+} substitution.

In this perspective, systematic *in situ* X-ray absorption studies of REE on other natural FAP could provide more information on the hydrothermal-magmatic fluids or be used as a geothermometer, which could lead to a major re-interpretation of geochemical processes and crystallisation conditions (Krneta *et al.*, 2018). This could also make it possible to decipher the effect of extrinsic (*e.g.*, temperature, source fluids) and intrinsic (*e.g.*, crystal-chemical) variables on REE patterns (Rakovan *et al.*, 2001; Borst *et al.*, 2020).

For sedimentary FAP, the assumptions for Y speciation, which include either mixed “Y(2) + Y-ads” speciation or the “Y(2) + carbonates” speciation, are both compatible with an adsorption-diffusion-substitution process (Koepfenkastrof and de Carlo, 1992). Both models can explain why REE in carbonated-FAP show a normalised pattern without fractionation, characterised by HREE enrichment so-called “past seawater pattern” (Reynard *et al.*, 1999). The Y(2) + carbonate model is particularly relevant because REE are mainly complexed by carbonate groups in seawater, which also shows a HREE-enriched pattern (Schijf and Byrne, 2021). We thus assume that the conservative (*i.e.* without fractionation) REE uptake in FAP is likely to be promoted by carbonate complexation, where both REE and carbonates are trapped in the FAP lattice during early diagenesis by their direct uptake from the hydrated layer (Cazalbou *et al.*, 2004). Since REE and carbonates are mainly enriched concomitantly in a strongly distorted crystal fringe located in the outer edges of FAP nanocrystallites (Liao *et al.*, 2019; in agreement with our EXAFS results), the crystal chemistry effect on the partitioning is inhibited while the effect of the fluid complexation (*i.e.* REE carbonate ions in seawater or porewater) is predominantly recorded, which likely implies non-Henry’s Law behaviour for the REE partitioning in S-FAP (Pan *et al.*, 2003).

Therefore, *in situ* X-ray absorption studies of REE could be applied to marine geochemistry to estimate whether overprinting of REE FAP fractionation has occurred, and whether a reliable seawater-porewater signature is preserved. This is particularly valuable for examining temporally laminated structures containing FAP, such as phosphorite grains or some polymetallic nodules, used to unravel past seawater conditions and their

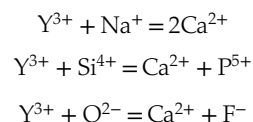
temporal changes like pH, redox, or ocean circulation (Kocsis *et al.*, 2016).

Conclusions

We studied the speciation of yttrium, a geochemical proxy for HREE, in hydrothermal and sedimentary FAP minerals using X-ray absorption spectroscopy. Analyses of Y K-edge XANES and EXAFS spectra, including *ab initio* calculations, shell fitting, wavelet analysis and linear combination show that:

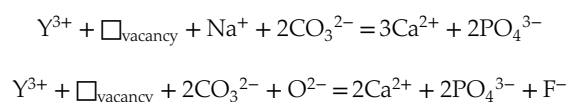
- 1) Y exclusively substitutes for Ca in the Ca(2) site in the hydrothermal Durango FAP;
- 2) Y can be found either as a mixture of Ca(2) substituted and inner shell tridentate adsorbate in the c axis channel in sedimentary FAP, or as substitution for the Ca(2) site with coupled substitution of a carbonate group in the direct surrounding atomic environment in B-type carbonated FAP.

Regardless of the FAP origin, the charge compensation mechanism is likely to be based on coupled substitutions such as:



Although the latter substitutions were not distinguished by our approach, we excluded the $2Y^{3+} + \square_{vacancy} = 3Ca^{2+}$ substitution due to the failure to detect Y or other heavy elements in the nearest atomic shell around Y.

For the sedimentary B-type carbonated FAP, we suggest that the following substitutions are likely to occur:



Regardless of geological context, Y speciation provides crucial information for a better understanding of REE partitioning and the geochemical information derived from it.

Acknowledgments

Work carried out within the framework of the scientific co-operation agreement between the Mohammed VI Polytechnic University, the University of Montpellier and the Centre National de la Recherche Scientifique [Specific Agreement n°UM190775 on “The multi-scale distribution of minor and trace elements in Moroccan phosphate basins”]. We also acknowledge the European Synchrotron Radiation Facility for provision of synchrotron radiation facilities. We thank Bernard Fraisse for his technical assistance with the XRD measurements at the RRXG platform (Réseau des Rayons X et Gamma) of University of Montpellier (Montpellier, France). We would also like to thank Valérie Magnin for her contribution to the micro-XRF data carried out at the ISTerre laboratory (Grenoble, France).

Editor: Satish Myneni

Author Contributions

JLB and AE participated in the sediment sampling strategy. VMR carried out the acquisition and processing of the LIBS data. JA provided FTIR measurements. CB carried out the XRF and XRD measurements. CB, MM and OM performed XANES and EXAFS acquisitions which were then processed by CB and MM. CB and MM wrote the manuscript. All authors participated to discussions.

Additional Information

Supplementary Information accompanies this letter at <https://www.geochemicalperspectivesletters.org/article2326>.



© 2023 The Authors. This work is distributed under the Creative Commons Attribution Non-Commercial No-Derivatives 4.0

License, which permits unrestricted distribution provided the original author and source are credited. The material may not be adapted (remixed, transformed or built upon) or used for commercial purposes without written permission from the author. Additional information is available at <https://www.geochemicalperspectivesletters.org/copyright-and-permissions>.

Cite this letter as: Bonnet, C., Muñoz, M., Mathon, O., Motto-Ros, V., Elghali, A., Parat, F., Aubineau, J., Bodinier, J.-L. (2023) Sorption model for yttrium in fluorapatite: Geochemical implications. *Geochem. Persp. Let.* 27, 1–7. <https://doi.org/10.7185/geochemlet.2326>

References

- AUBINEAU, J., PARAT, F., ELGHALI, A., RAJI, O., ADDOU, A., BONNET, C., MUÑOZ, M., MAUGUIN, O., BARON, F., JOUTI, M.B., YAZAMID, O.K., BODINIER, J.-L. (2022) Highly variable content of fluorapatite-hosted CO₃²⁻ in the Upper Cretaceous/ Paleogene phosphorites (Morocco) and implications for paleodepositional conditions. *Chemical Geology* 597, 120818. <https://doi.org/10.1016/j.chemgeo.2022.120818>
- BLUNDY, J., WOOD, B. (2003) Partitioning of trace elements between crystals and melts. *Earth and Planetary Science Letters* 210, 383–397. [https://doi.org/10.1016/S0012-821X\(03\)00129-8](https://doi.org/10.1016/S0012-821X(03)00129-8)
- BORISOV, S.V., KLEVTŠOVA, R.F. (1963) The crystal structure of TR-Sr-apatite. *Journal of Structural Chemistry* 4, 575–577. <https://doi.org/10.1007/BF00747639>
- BORST, A.M., FINCH, A.A., FRIIS, H., HORSBURGH, N.J., GAMALETOS, P.N., GOETTLICHER, J., STEININGER, R., GERAKI, K. (2020) Structural state of rare earth elements in eudialyte-group minerals. *Mineralogical Magazine* 84, 19–34. <https://doi.org/10.1180/mgm.2019.50>
- CAZALBOU, S., EICHERT, D., DROUET, C., COMBES, C., REY, C. (2004) Minéralisations biologiques à base de phosphate de calcium. *Comptes Rendus Palevol* 3, 563–572. <https://doi.org/10.1016/j.crvp.2004.07.003>
- CHEN, N., PAN, Y., WEIL, J.A. (2002) Electron paramagnetic resonance spectroscopic study of synthetic fluorapatite: Part I. Local structural environment and substitution mechanism of Gd³⁺ at the Ca₂ site. *American Mineralogist* 87, 37–46. <https://doi.org/10.2138/am-2002-0105>
- CHERNIAK, D.J. (2000) Rare earth element diffusion in apatite. *Geochimica et Cosmochimica Acta* 64, 3871–3885. [https://doi.org/10.1016/S0016-7037\(00\)00467-1](https://doi.org/10.1016/S0016-7037(00)00467-1)
- EMSBÖ, P., MCLAUGHLIN, P.I., BREIT, G.N., DU BRAY, E.A., KOENIG, A.E. (2015) Rare earth elements in sedimentary phosphate deposits: Solution to the global REE crisis? *Gondwana Research* 27, 776–785. <https://doi.org/10.1016/j.gr.2014.10.008>
- FAUCHER, M., PANNETIER, J. (1980) Refinement of the Y₂O₃ structure at 77 K. *Acta Crystallographica Section B* 36, 3209–3211. <https://doi.org/10.1107/S0567740880011351>
- FLEET, M.E., PAN, Y. (1995) Site preference of rare earth elements in fluorapatite. *American Mineralogist* 80, 329–335. <https://doi.org/10.2138/am-1995-3-414>
- GLEASON, J.D., MARIKOS, M.A., BARTON, M.D., JOHNSON, D.A. (2000) Neodymium isotopic study of rare earth element sources and mobility in hydrothermal Fe oxide (Fe-P-REE) systems. *Geochimica et Cosmochimica Acta* 64, 1059–1068. [https://doi.org/10.1016/S0016-7037\(99\)00325-7](https://doi.org/10.1016/S0016-7037(99)00325-7)
- HUGHES, J.M., CAMERON, M., CROWLEY, K.D. (1990) Crystal structures of natural ternary apatites: Solid solution in the Ca₅(PO₄)₃X (X = F, OH, Cl) system. *American Mineralogist* 75, 295–304. http://www.minsocam.org/ammin/AM75/AM75_295.pdf
- HUGHES, J.M., CAMERON, M., MARIANO, A.N. (1991) Rare-earth-element ordering and structural variations in natural rare-earth-bearing apatites. *American Mineralogist* 76, 1165–1173. http://www.minsocam.org/ammin/AM76/AM76_1165.pdf
- KASHIWABARA, T., TODA, R., NAKAMURA, K., YASUKAWA, K., FUJINAGA, K., KUBO, S., NOZAKI, T., TAKAHASHI, Y., SUZUKI, K., KATO, Y. (2018) Synchrotron X-ray spectroscopic perspective on the formation mechanism of REY-rich muds in the Pacific Ocean. *Geochimica et Cosmochimica Acta* 240, 274–292. <https://doi.org/10.1016/j.gca.2018.08.013>
- KHUDOLOZHKIN, V.O., URUSOV, V.S., TOBELKO, K.I., VERNADSKIY, V.I. (1973) Dependence of structural ordering of rare earth atoms in the isomorphous series apatite-britholite (abukumalite) on composition and temperature. *Geochemical International* 10, 1171–1177.
- KIS, V.K., CZIGÁNY, Z., DALLOS, Z., NAGY, D., DÓDONY, I. (2019) HRTEM study of individual bone apatite nanocrystals reveals symmetry reduction with respect to P6₃/m apatite. *Materials Science and Engineering: C* 104, 109966. <https://doi.org/10.1016/j.msec.2019.109966>
- KOCSIS, L., GHEERBRANT, E., MOUFLIH, M., CAPPETTA, H., ULIANOV, A., CHIARADIA, M., BARDET, N. (2016) Gradual changes in upwelled seawater conditions (redox, pH) from the late Cretaceous through early Paleogene at the northwest coast of Africa: Negative Ce anomaly trend recorded in fossil bio-apatite. *Chemical Geology* 421, 44–54. <https://doi.org/10.1016/j.chemgeo.2015.12.001>
- KOEPPENKASTROP, D., DE CARLO, E.H. (1992) Sorption of rare-earth elements from seawater onto synthetic mineral particles: An experimental approach. *Chemical Geology* 95, 251–263. [https://doi.org/10.1016/0009-2541\(92\)90015-W](https://doi.org/10.1016/0009-2541(92)90015-W)
- KRNETA, S., CIOBANU, C.L., COOK, N.J., EHRIG, K.J. (2018) Numerical Modeling of REE Fractionation Patterns in Fluorapatite from the Olympic Dam Deposit (South Australia). *Minerals* 8, 342. <https://doi.org/10.3390/min8080342>
- LIAO, J., SUNA, X., LI, D., SAE, R., LUB, Y., LIN, Z., XUB, L., ZHANG, R., PANG, Y., XU, H. (2019) New insights into nanostructure and geochemistry of bioapatite in REE-rich deep-sea sediments: LA-ICP-MS, TEM, and Z-contrast imaging studies. *Chemical Geology* 512, 58–68. <https://doi.org/10.1016/j.chemgeo.2019.02.039>
- MACKIE, P.E., YOUNG, R.A. (1973) Location of Nd dopant in fluorapatite, Ca₅(PO₄)₃F: Nd. *Journal of Applied Crystallography* 6, 26–31. <https://doi.org/10.1107/S0021889873008009>
- MUÑOZ, M., ARGOUL, P., FARGES, F. (2003) Continuous Cauchy wavelet transform analyses of EXAFS spectra: A qualitative approach. *American Mineralogist* 88, 694–700. <https://doi.org/10.2138/am-2003-0423>



- NI, Y., HUGHES, J.M., MARIANO, A.N. (1995) Crystal chemistry of the monazite and xenotime structures. *American Mineralogist* 80, 21–26. <https://doi.org/10.2138/am-1995-1-203>
- PAN, Y., FLEET, M.E. (2002) Compositions of the Apatite-Group Minerals: Substitution Mechanisms and Controlling Factors. *Reviews in Mineralogy and Geochemistry* 48, 13–49. <https://doi.org/10.2138/rmg.2002.48.2>
- PAN, Y., DONG, P., CHEN, N. (2003) Non-Henry's Law behavior of REE partitioning between fluorapatite and CaF₂-rich melts: Controls of intrinsic vacancies and implications for natural apatites. *Geochimica et Cosmochimica Acta* 67, 1889–1900. [https://doi.org/10.1016/S0016-7037\(02\)01285-1](https://doi.org/10.1016/S0016-7037(02)01285-1)
- RAGNARSDOTTIR, K.V., OELKERS, E.H., SHERMAN, D.M., COLLINS, C.R. (1998) Aqueous speciation of yttrium at temperatures from 25 to 340°C at P_{sat} : an in situ EXAFS study. *Chemical Geology* 151, 29–39. [https://doi.org/10.1016/S0009-2541\(98\)00068-0](https://doi.org/10.1016/S0009-2541(98)00068-0)
- RAKOVAN, J., NEWVILLE, M., SUTTON, S. (2001) Evidence of heterovalent europium in zoned Llagua apatite using wavelength dispersive XANES. *American Mineralogist* 86, 697–700. <https://doi.org/10.2138/am-2001-5-610>
- REYNARD, B., LÉCUYER, C., GRANDJEAN, P. (1999) Crystal-chemical controls on rare-earth element concentrations in fossil biogenic apatites and implications for paleoenvironmental reconstructions. *Chemical Geology* 155, 233–241. [https://doi.org/10.1016/S0009-2541\(98\)00169-7](https://doi.org/10.1016/S0009-2541(98)00169-7)
- SCHIFF, J., BYRNE, R.H. (2021) Speciation of yttrium and the rare earth elements in seawater: Review of a 20-year analytical journey. *Chemical Geology* 584, 120479. <https://doi.org/10.1016/j.chemgeo.2021.120479>
- URUSOV, V.S., KHUDOLOZHKIN, V.O. (1974) An energy analysis of cation ordering in apatite. *Geochemistry International* 11, 1048–1053.